Composites Part A

The effects of alkaline digestion, bleaching and ultrasonication treatment of fibre on 3D printed harakeke fibre reinforced polylactic acid composites

--Manuscript Draft--

Figure 1

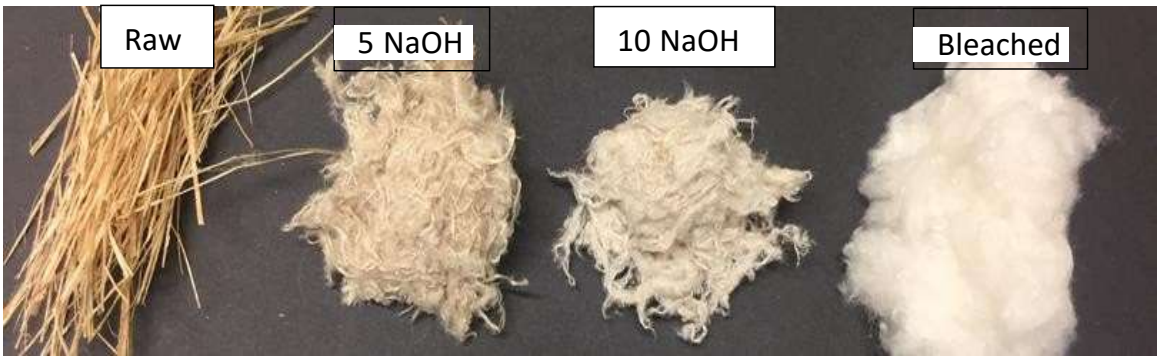

Figure 2

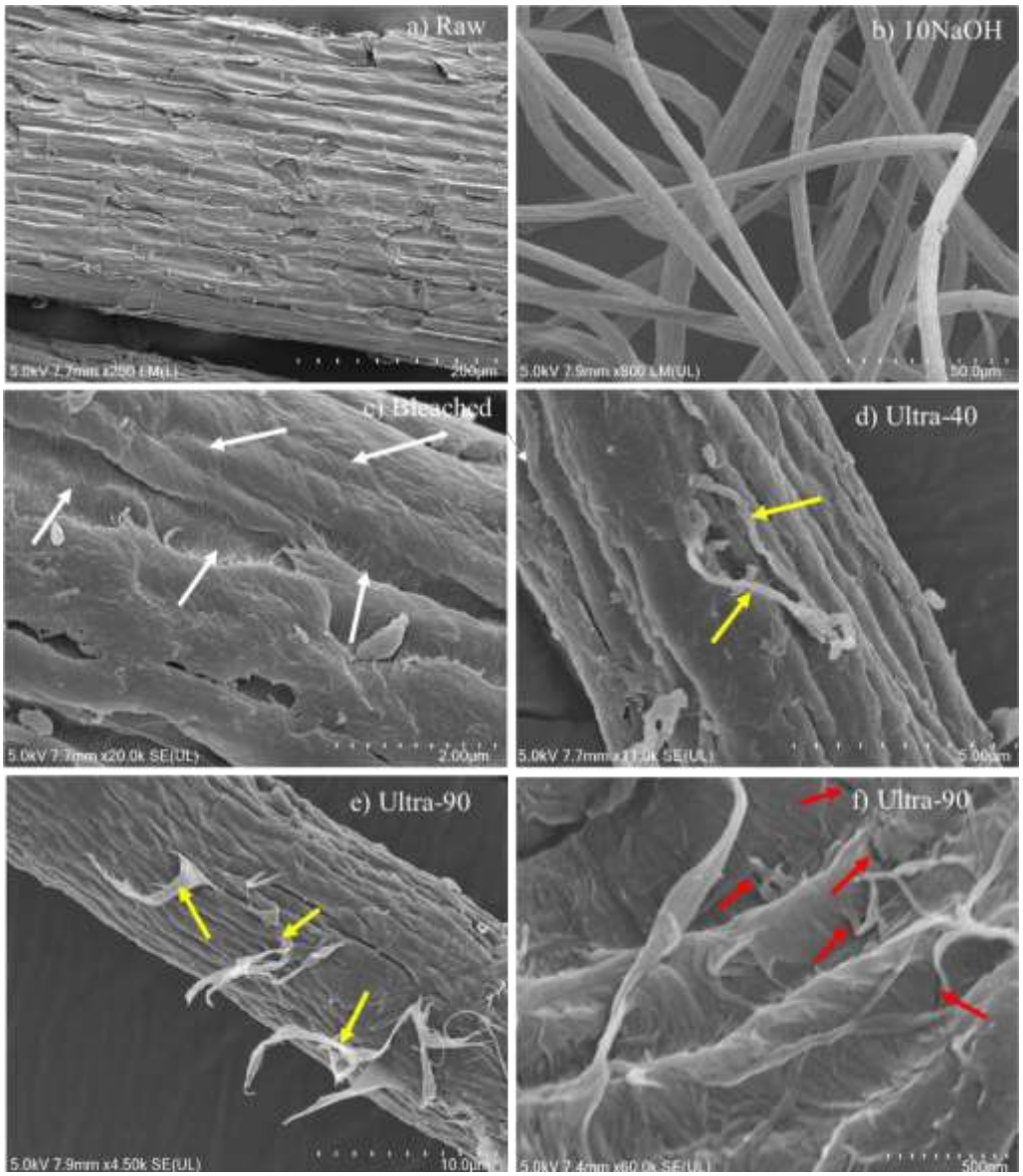

Figure 3

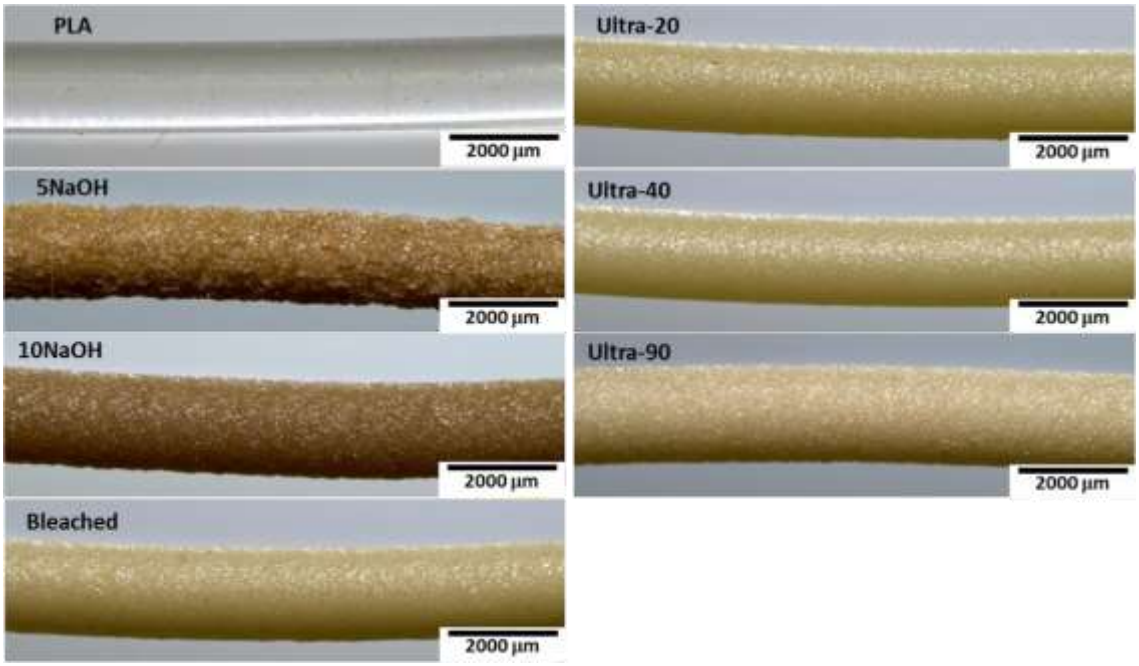
PLA
2000 µm
Ultra-20
2000 µm
5NaOH
2000 µm
Ultra-40
2000 µm
10NaOH
2000 µm
Ultra-90
2000 µm
Bleached
2000 µm

Figure 4

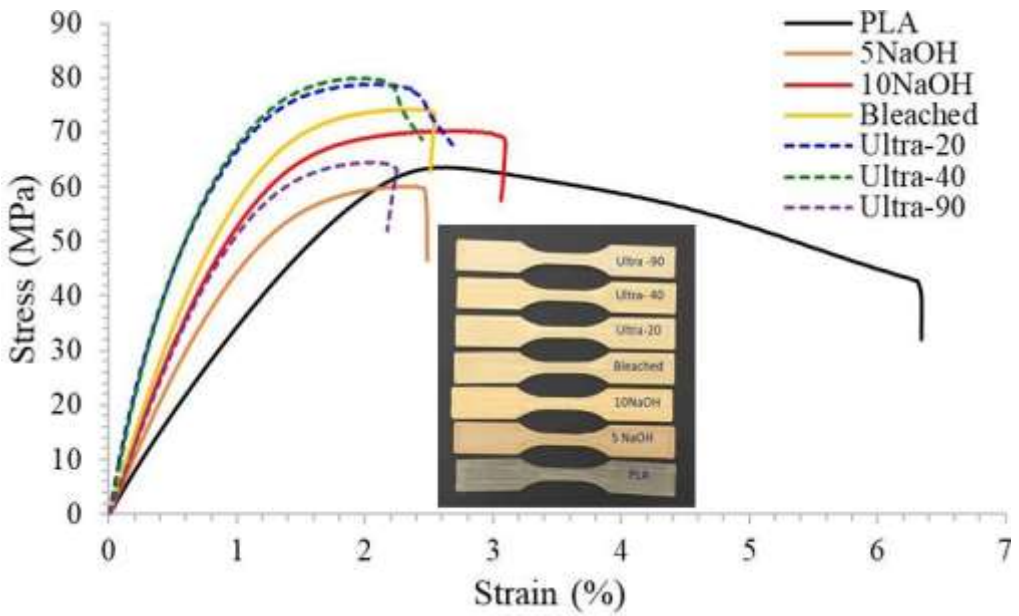
Stress (MPa)
Strain (%)
PLA
5NaOH
10NaOH
Bleached
Ultra-20
Ultra-40
Ultra-90
Ultra -90
Ultra- 40
Ultra-20
Bleached
10NaOH
5 NaOH
PLA

Figure 5

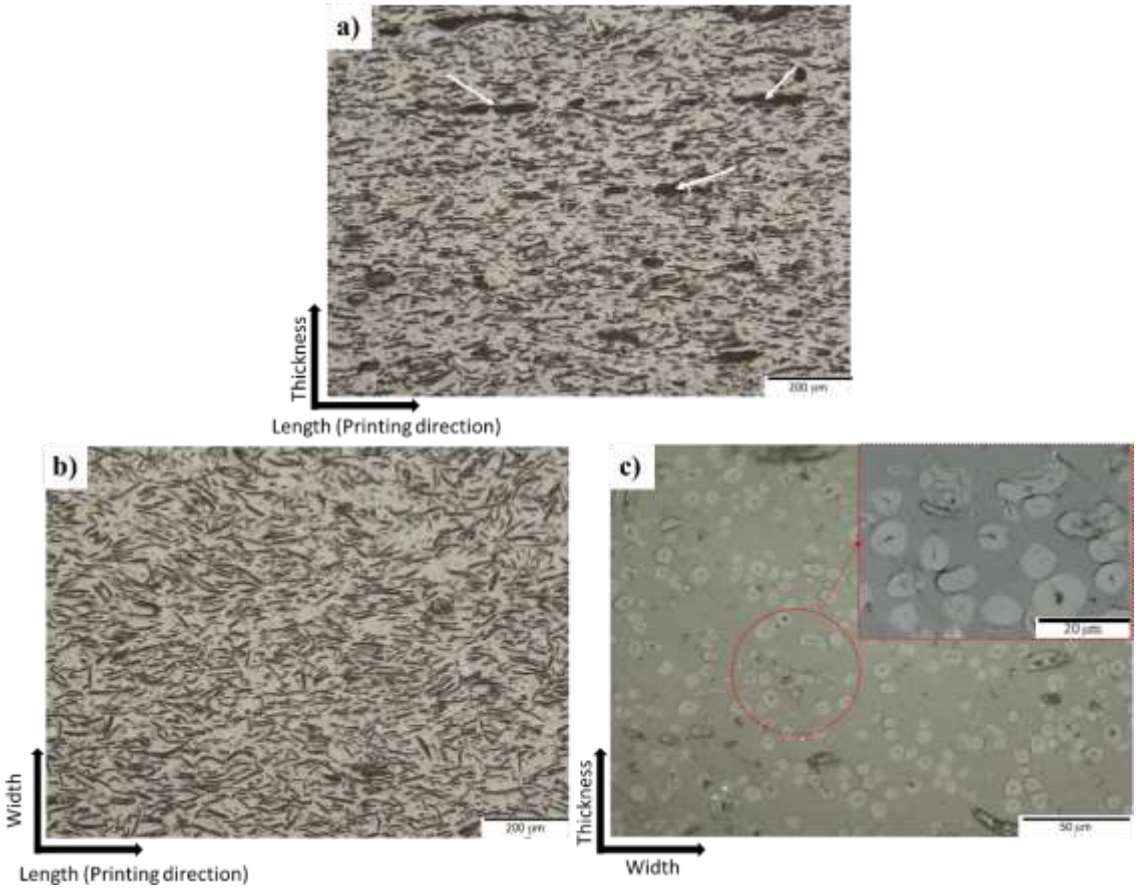
a)
Thickness
Length (Printing direction)
b)
Width
Length (Printing direction)
c)
Thickness
Width

Figure 6

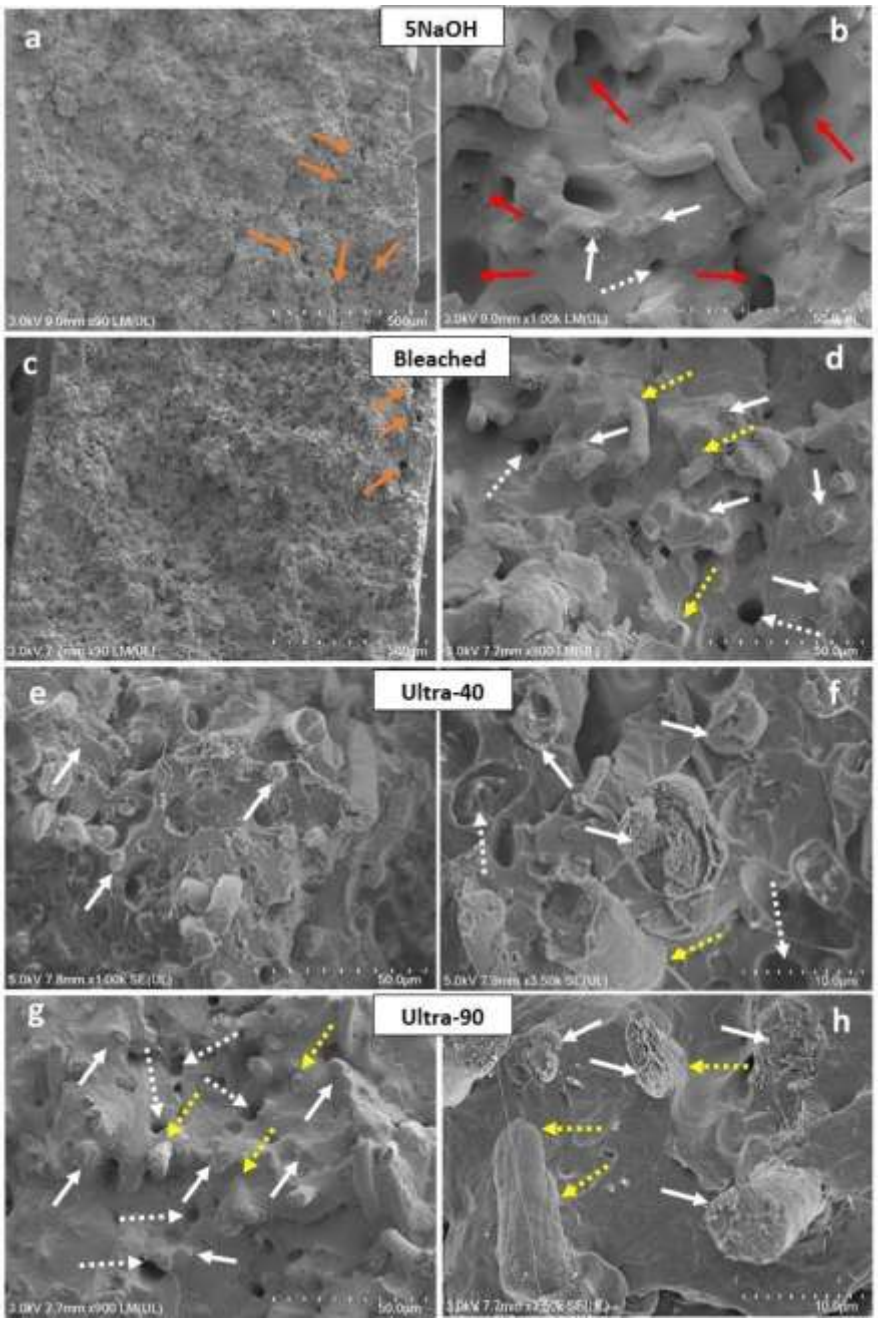

Figure 7

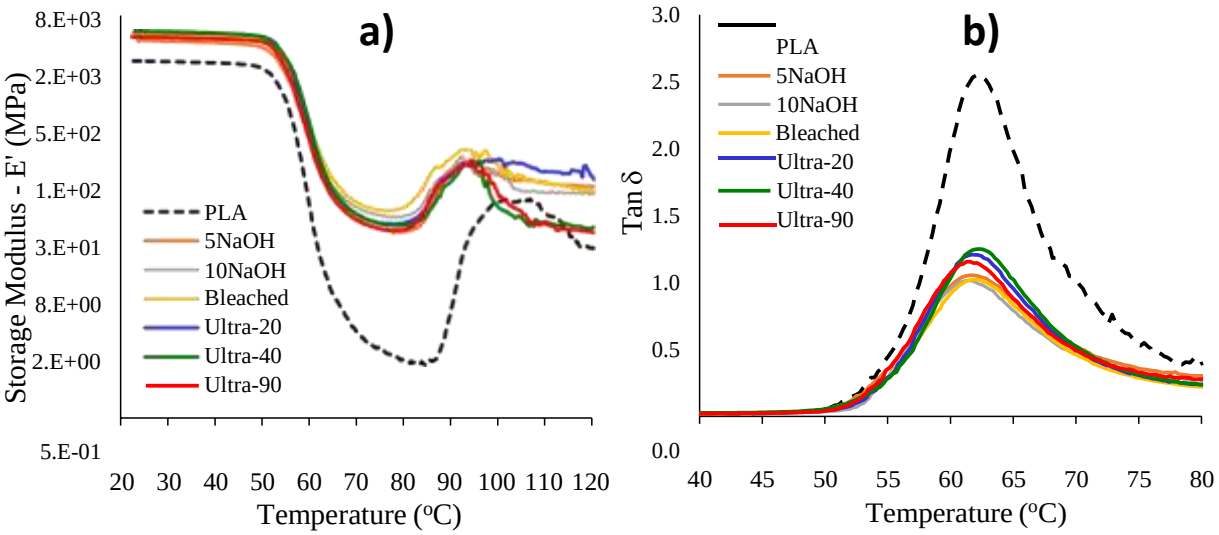
a)
Storage Modulus - E' (MPa)
8.E+03
2.E+03
5.E+02
1.E+02
3.E+01
8.E+00
2.E+00
5.E-01
20 30 40 50 60 70 80 90 100 110 120
Temperature (°C)
PLA
5NaOH
10NaOH
Bleached
Ultra-20
Ultra-40
Ultra-90
b)
Tan δ
3.0
2.5
2.0
1.5
1.0
0.5
0.0
40 45 50 55 60 65 70 75 80
Temperature (°C)
PLA
5NaOH
10NaOH
Bleached
Ultra-20
Ultra-40
Ultra-90

Figure captions

Figure 1: Photograph of as-received raw harakeke fibre and treated fibres.

Figure 2: SEM of raw fibre bundles (a), fibre after alkaline treatment (b), bleaching (c), and ultrasonication for 40 min (d) and 90 min (e, f). The white arrows indicate the microfibrils on the bleached fibres; the yellow arrows show the defibrillation caused by the sonication process; the red arrows indicate the micro cracks formed in the fibres with excessive sonication time.

Figure 3: Stereo microscopy images of filaments of neat PLA and composites with fibre subjected to different treatments.

Figure 4: Stress-strain curves (in tension) of 3D printed samples and the images of 3D printed samples

Figure 5: Optical microscopy images of 3D printed harakeke-PLA composite (bleached). The images were taken from the cross-section of the tensile specimen free span. The white arrows indicate the inter layer defects.

Figure 6: SEM images of the fracture surface of 3D printed composites. Orange arrows indicate interlayer defects, Red arrows indicate pull-out of fibre bundles, white dotted arrows indicate single fibre pull out, white arrows indicate fibre breakage, yellow dotted arrows indicate good wetting/bonding.

Figure 7 - Storage modulus (a) and tan δ (b) obtained from DMA tests of 3D printed samples of PLA and the composites with harakeke fibres.

Tables

Table 1 – Sample identification and corresponding fibre treatment used in each composite formulation. All PLA composites were produced using 30 wt% of fibres.

Sample ID	Fibre treatment
5NaOH	Digested with 5% NaOH and 2% Na_2SO_3
10NaOH	Digested with 10% NaOH and 2% Na_2SO_3
Bleached	10NaOH fibre bleached with 5% H_2O_2
Ultra-20	Bleached fibre ultrasonicated for 20 min
Ultra-40	Bleached fibre ultrasonicated for 40 min
Ultra-90	Bleached fibre ultrasonicated for 90 min

Table 2: Average fibre dimensions (bundle/elementary fibre) length and diameter of raw and treated harakeke fibres

ID	Fibre Composition					Fibre dimension		
	Acid insoluble lignin (%)	Acid soluble lignin (%)	Total lignin (%)	Hemi-cellulose (%)	Cellu-lose (%)	Length (mm)	Diameter (µm)	Aspect ratio
Raw	13.36	2.48	15.83	18.80	46.00	300	280	-
5NaOH	2.73	0.64	3.37	10.85	77.30	1.60	9.50	168
10NaOH	1.69	0.54	2.23	3.20	88.15	1.38	7.30	189
Bleached	1.33	0.59	1.82	2.30	92.60	1.29	6.92	186

Table 3: Data for XRD and TGA analysis of fibre.

Fibre Type	XRD		TGA		
	Crystallinity Index (%)	Crystallite size (Å)	T_{onset} (°C)	T_d (°C)	Residual (%) at 600 °C
Raw	72.8	21.2	255	357	20.1
5 NaOH	79.7	37.2	326	361	14.3
10 NaOH	81.5	41.2	334	355	12.2
Bleached	82.2	43.9	333	362	12.1

* T_{onset} is the onset temperature of degradation and T_d is the temperature of maximum degradation rate.

Table 4: Onset temperature and decomposition temperature of filament with different treated fibre

Composite	PLA	5NaOH	10NaOH	Bleached	Ultra-20	Ultra-40	Ultra-90
T_{onset} (ºC)	337	292	308	324	329	327	323
T_d (ºC)	356	325	328	341	346	343	341

* T_{onset} is the onset temperature of degradation and T_d is the temperature of maximum degradation rate.

Table 5: Tensile properties of 3D printed 30 (wt)% fibre composites and PLA. The coefficient of variation (COV) is presented in parentheses. Similar letters (a, b, or c) indicate that there is no statistical difference between formulations.

Formulation	**UTS (MPa)**	**E (GPa)**	**ε_{break} (%)**
PLA	65.25 (0.02)^{c,d}	3.46 (0.04)^{d}	6.67 (0.04)^{a}
5NaOH	61.81 (0.03)^{d}	5.65 (0.09)^{c}	2.20 (0.10)^{b,c}
10NaOH	70.44 (0.02)^{b,c}	6.39 (0.04)^{b,c}	2.42 (0.14)^{b}
Bleached	75.47 (0.05)^{a,b}	7.21 (0.09)^{b}	2.25 (0.10)^{b,c}
Ultra-20	78.40 (0.02)^{a}	8.36 (0.06)^{a}	2.23 (0.11)^{b,c}
Ultra-40	79.33 (0.07)^{a}	8.69 (0.10)^{a}	1.82 (0.14)^{c}
Ultra-90	64.40 (0.08)^{c,d}	6.35 (0.13)^{b,c}	2.11 (0.10)^{b,c}

UTS – Ultimate tensile strength; E – Young's modulus; ε_{break} – Strain at break.

Table 6 - Summary of DMA results of 3D printed samples with different formulations. The values are the average of two tested samples per condition.

Condition	E' 25 ºC (MPa)	E' 60 ºC (MPa)	E' 80 ºC (MPa)	Max. Tan δ	T_g (ºC)*
PLA	2,870	121	2.87	2.59	62.21
5NaOH	4,478	456	43.34	1.06	61.64
10NaOH	5,504	566	70.26	1.02	61.43
Bleached	5,483	668	69.34	1.08	62.13
Ultra-20	5,689	635	54.42	1.22	61.81
Ultra-40	5,880	670	54.25	1.23	62.15
Ultra-90	5,187	515	50.24	1.13	61.53

* T_g considered as the temperature of maximum Tan δ

Table 7 – Summary of DSC results of 3D printed samples during the first and second heating cycles.

		Tg (ºC)	Tcc (ºC)	ΔHcc (J/g)	Tm1 (ºC)	Tm2 (ºC)	ΔHm (J/g)	Xc (%)
PLA	1st run	60.2	114.3	-26.8	152.4		27.1	0.87
	2nd run	63.7	117.5	-26.4	150.6		26.9	0.57
5NaOH	1st run	65.9	114.0	-31.6	150.6	155.8	36.1	4.95
	2nd run	63.3	119.5	-32.8	151.2	-	32.7	0.03
10NaOH	1st run	65.3	113.8	-29.9	150.5	155.0	34.5	4.94
	2nd run	63.4	120.8	-30.3	151.7	-	30.7	0.40
Bleached	1st run	62.3	109.9	-23.6	150.3	-	31.0	7.93
	2nd run	63.5	119.9	-29.0	151.1	-	29.5	0.52
Ultra-20	1st run	63.3	112.5	-22.5	151.7	-	30.9	9.07
	2nd run	64.3	120.7	-23.4	151.8	-	23.9	0.61
Ultra-40	1st run	62.2	111.3	-22.4	151.3	-	28.3	6.39
	2nd run	64.5	120.5	-23.1	151.6	-	23.5	0.42
Ultra-90	1st run	64.8	112.2	-29.3	150.3	154.6	32.9	3.87
	2nd run	63.4	116.9	-31.1	150.8	-	31.6	0.54

Tcc – Cold crystallization temperature; Tg – Glass transition temperature; Tm – Melting temperature; ΔHcc – Cold crystallization heat; ΔHm – Heat of melting; Xc – PLA crystallinity

CREDIT AUTHOR STATEMENT

M. D. H. Beg – Conceptualization, Investigation, Methodology, Writing-Original Draft

K. L. Pickering – Supervision, Funding acquisition, Writing-Review & Editing

1 August, 2022

The effects of alkaline digestion, bleaching and ultrasonication treatment of fibre on 3D printed harakeke fibre reinforced polylactic acid composites

M. D. H. Beg*, K. L. Pickering, and C. Gauss

School of Engineering, Division of Health, Engineering, Computing & Science, The University of Waikato, Private Bag 3105, Hamilton, New Zealand.

Abstract

This paper documents an investigation of the effects of fibre treatment on New Zealand flax (harakeke) fibre reinforced polylactic acid (PLA) composites. The raw fibre was alkali digested, followed by bleaching and then modified with ultrasonication. Alkali treatment removed lignin and other non-cellulosic components and partially separated fibre bundles while bleaching further removed lignin and improved the separation of elementary fibres, resulting in microfibres with a cellulose content 92 wt%. With subsequent ultrasonication, microfibrils could be seen partially separated (defibrillation) at fibre surfaces. Treated fibres were compounded with PLA at a fibre loading of 30 wt% and extruded into composite filaments. Filaments from alkali, bleached and ultrasonication-treated fibres had smooth surfaces, which translated into high-quality printability along with good mechanical performance. The combination of chemically treated microfibres with selective surface defibrillation using ultrasonication and fibre alignment induced by the printing process resulted in 3D printed samples with a tensile strength of 79 MPa and Young's modulus of 8.7 GPa, which are the highest values reported so far for 3D printed PLA-based composites reinforced with short fibres.

Keywords: **A. Biocomposites; B. Interface/interphase; D. Mechanical testing; E. 3-D Printing**

* Corresponding Author: M.D.H. Beg, Email: mdhbeg@waikato.ac.nz Phone: +64211373480

1. Introduction

Additive manufacturing (AM) has become one of the most promising techniques for fabricating parts with complex shapes due to its cost-saving, high production efficiency and integrated manufacturing [1,2]. Among the numerous AM methods, fused deposition modelling (FDM) is one of the most widely used approaches to manufacture conceptual prototypes and common parts [3,4]. The use of bio-derived materials in additive manufacturing continues to increase with the constant demand for innovation in

sustainable materials and circular economy requirements in the manufacturing sector [5]. Among different matrices, poly (lactic acid), also known as polylactide (PLA), is a common filament feedstock material for FDM because of its renewability and biodegradability. The main problem in FDM for printed composites is inherent extrusion-induced defects, such as porosity caused by poor interfacial bonding between fibre and matrices [6] which limits the mechanical properties, especially at higher fibre contents. Recently, Xianglian et al. studied 3D printed hemp hurd fibre PLA composites with fibre loading up to 40wt%; however, both the tensile strength and flexural strength decreased significantly after 10-20wt% fibre loading [7] due to an increase in porosity and the associated inadequate interfacial bonding. Milosevic et al. studied 3D printed hemp and harakeke fibre reinforced recycled polypropylene (PP) composites and Stoof et al. studied 3D printed hemp and harakeke/PLA composites; both studies found a reduction in tensile strength at 30wt% fibre loading due to lack of bonding between the printed layers and associated voids [8,9].

To help overcome this problem, natural fibre surfaces can be modified by mechanical, chemical, or physical techniques before composite fabrication. Alkali treatment is one of the most common chemical treatment methods to modify the surface of natural fibre to improve interfacial bonding and lower surface tension. Alkali treatment reduces the fibre diameter by removing amorphous materials from the fibre surface such as hemicellulose, lignin, and pectin, increasing the aspect ratio of the fibres [10]. In addition, alkaline treatment increases the roughness of the fibres, surface area, and affects the degree of polymerisation and orientation of the cellulose crystallites [11,12]. These attributes generally improve the fibre/matrix interfacial shear strength (IFSS), leading to composites with better mechanical performance, and the removal of amorphous materials improves the thermal stability of the fibres and composites [10]. [13]

Bleaching of fibres also has the potential to remove lignin on the surface and within the fibres, thereby exposing more cellulose. Bleaching can be done using various chemicals, including oxygen, chlorine, chlorine dioxide, hypochlorite and hydrogen peroxide [14]. Among them, hydrogen peroxide bleaching is considered the most environmentally friendly solution as it does not use any chlorine-based chemicals.

Ultrasonication is another environmentally friendly technique for modifying fibre morphology which can remove amorphous materials from the fibre surface, causing etching effects on the fibre

surface [15]. The effect of ultrasonication in degrading the bonding between cellulose and amorphous materials on the surface of fibre has been reported [16–18]. Moshiul Alam et al. [19] studied the simultaneous effects of both alkali and ultrasonication treatments on oil palm empty fruit bunch fibre reinforced PLA composites and observed a significant improvement in the mechanical, thermal and interfacial properties of the resultant composites.

Although some literature is available on alkali treatment, bleaching or ultrasonication treatment of natural fibre for composites, no systematic study has been found for mechanical and thermomechanical properties of 3D printed composites where the combined effects of fibre treatment has been investigated. This work aims to address that, utilising harakeke (New Zealand flax) as a sustainable fibre to reinforce PLA in 3D printed composites, where alkali treatment, bleaching and ultrasonication fibre treatments were used to improve the mechanical and thermomechanical properties of composites.

2. Experimental

2.1. Materials

Harakeke *(Phormium tenax)* fibre was supplied by Templeton Flax Milling Heritage Trust, New Zealand. The bulk sodium hydroxide (reagent grade, ≥ 98%), sodium sulphite (reagent grade, ≥ 98%), and hydrogen peroxide (30%), were supplied by Sigma-Aldrich, New Zealand. PLA grade 2003D with melt flow index (MFI) of 6 g/10 min (210°C, 2.16kg) and specific gravity of 1.24 g.cm^{-3} was purchased from Nature Works® (Plymouth, MN, United States).

2.2. Fibre Treatment

Long harakeke fibres (1-1.5 m long) were oven dried at 80 ºC for 48 h and cut into 2-3 cm lengths by a guillotine. Approximately 240 g of fibres were placed in three stainless steel canisters (80 g in each canister) with pre-mixed solutions of 5% or 10% NaOH and 2% Na_2SO_3 (by weight). The canisters were then inserted into a custom made laboratory-scale batch digester. The system was heated from 25 °C (room temperature) to 160 °C over 2 hours and then holding the temperature at 160 °C for 2 hours. Digestion took place with a 1:8 ratio of fibre to solution (by weight). After completing the cycle the system was quenched to approximately 50 °C. After treatment, the fibres were thoroughly washed using tap water (until the pH reached 7). Fibres were then dried at 80ºC for 48 h. The fibre digested using 10% NaOH was further bleached using a solution based on hydrogen peroxide (H_2O_2). Initially, 3 L of distilled water was placed in a beaker and heated up to 70 ºC then 45 g of digested fibre was placed in the

beaker and stirred. Then, 150 ml H_2O_2 (5% by volume) was added to the beaker. The bleaching process was continued for 10 min on the heating plate, with continuous manual stirring using a glass stirring rod. The bleached fibre was washed using tap water until a pH of 7 was achieved and then dried in the oven for 48 h at 80 °C. The bleached fibre was treated further using a QSONICA Sonicator (Newtown, CT, United States) at 20 kHz; about 4 g of dried fibre was placed in a 1000 mL beaker with 800 mL of distilled water and after keeping the beaker in an ice bath for 10 min to cool down to 10 °C, it was placed under an ultrasonication horn with a horn diameter of 25.4 mm. Ultrasonication was carried out in cycles (30 s on and 5 s off) for 10 min. Then the beaker was taken out from the ultrasonic chamber and placed in the ice bath again to cool down. The process was repeated to reach the ultrasonication treatment time of 20 min, 40 min, or 90 min. After treatment, the fibre was washed using tap water and then dried for 48 hrs at 80°C. After each treatment, the fibres were prone to clumping together upon drying and required separating before composite production. A domestic Sunbeam Multigrinder with blunt blades was used at a high rotational speed to shear the fibres apart.

2.3. Fibre Characterization

Klason lignin content was determined following TAPPI Standard T222 OM-02 and the acid-soluble lignin was determined following TAPPI Standard UM 250. Cellulose and hemicellulose contents were determined through wood sugar analysis by anion chromatography [20]. A detailed method description is included in the supplementary file M1.

Fibre length and diameter were measured from images obtained using an Olympus optical microscope model BX53 (Tokyo, Japan) equipped with polarized light. Over 100 fibres were analysed to get the average fibre length and diameter (some sample pictures are attached in the supplementary file; Fig. S1). Fibre surfaces were examined using a Hitachi S-4000 (Tokyo, Japan) field emission scanning electron microscope, operated at 5 kV. Samples were mounted with carbon tape on aluminium stubs and then sputter-coated with palladium to make them conductive prior to SEM observation. The X-ray diffraction (XRD) spectra were obtained using an Panalytical Empyrean XRD (Worcestershire, United Kingdom); fibres were chopped and pressed into a disk using a cylindrical steel mould before placing the sample onto the sample holder. The scanning range was used between 5° and 65° by employing CuKα radiation (λ=1.54 nm) with a voltage and current of 45 mV and 40 mA respectively. The cellulose

crystallinity index (*CrI*) of the fibres was calculated using the Segal method, according to the following equation [21]:

$$CrI = \frac{I002 - Iam}{I_{002}} \, x \, 100 \qquad (1)$$

where I_{002} is the maximum intensity of the (002) lattice diffraction peak of cellulose I, at a 2θ angle of approximately 22.7°, and I_{am} is the minimum intensity of diffraction at an angle of 18.3° representing amorphous content.

Thermogravimetric analysis (TGA) of different treated fibres was carried out using a Perkin Elmer simultaneous thermal analyser STA 8000 (Waltham, MA, United States). Data were obtained at a rate of 10 °C/min over a heating range of 30 °C to 600 °C under an argon flow of 40 mL/min.

2.4 Composite Fabrication

Composites were produced by melt compounding followed by filament extrusion and named according to the fibre treatment, as shown in Table 1. Firstly, the fibres and PLA were compounded in a batch process using a custom-made Sigma blade type compounder at 185 ºC and 30 rpm. For each batch, 50 g of PLA/fibre was compounded using a fibre content of 30 wt%. Initially, a predetermined amount of PLA was added slowly into the mixing chamber, then when the PLA melted completely and the measured torque became constant, the required amount of fibre was added slowly. After adding the fibres, compounding was continued for 10 min so that the torque became constant and the mixing was considered to be completed. After compounding, the composites were granulated into 3 mm particles using a Moretto GR knife mill (Mercer County, PA, Unites States). Then, the granules were dried in the vacuum oven at 60ºC for 2 h and extruded into filaments using a Filabot EX2 single screw extruder (Barre, Vermont, United States) at 180ºC. The extrusion and spooling speeds were adjusted to produce filaments with a constant diameter of 1.75 ± 0.10 mm. Samples for tensile testing and dynamic mechanical analysis (DMA) were 3D printed using a Maker Gear™ M2 desktop 3D printer (Beachwood, OH, Unites States) using the Simplify 3D® software package. Before printing, all the filaments were vacuum-dried for 2 h at 50 ºC. The samples were printed using the printing parameters as infill density 100%, nozzle diameter 0.75 mm, raster angle 0º (for all the layers), bed temperature 70ºC, nozzle temperature 210ºC, printing speed 1800 mm/min, and layer height 0.1 mm. The tensile samples were printed following ASTM D638 Type V specimens, with free-span nominal dimensions of 3.20 mm, 1.20 mm, and 11 mm for width, thickness, and length, respectively. After 3D printing, all the samples for

tensile tests, and DMA analysis were conditioned in a climatic chamber for 48 h at 23ºC and 50% relative humidity before testing.

2.5 Characterization of Composites

Tensile testing of the 3D printed samples was conducted using an Instron® 5982 universal testing machine (Norwood, MA, United States) equipped with a 5 kN load cell. The test was performed at a cross-head speed of 2 mm/min and an extensometer of 10 mm was used to measure the tensile strain. For each batch, five samples were tested to get the average values of tensile strength, Young's modulus and elongation at break. The mechanical testing results were analysed using the statistical software Minitab® 18 (Coventry, United Kingdom) using a one-way analysis of variance (ANOVA) test. The significant differences among averages were calculated using Tukey's method with a 95% of confidence. Dynamic mechanical analysis (DMA) was conducted using a Perkin Elmer DMA800 analyser (Waltham, MA, United States). This was performed in a single cantilever mode on 3D-printed prismatic (5mm x 1.5 mm x 30 mm) samples. The samples were subjected to dynamic strain from 22-140 ºC at 2 ºC/min, frequency of 1 Hz, and displacement amplitude of 50 µm. Differential Scanning Calorimetry (DSC) of the 3D printed samples was conducted using Netzch DSC3500 Differential Scanning Calorimeter (Selb, Germany) using aluminium crucibles from 20-200 ºC at 10 ºC/min under a nitrogen flow of 60 mL/min. The obtained thermograms were used to determine the glass transition (T_g), melting (T_m), and cold crystallization (T_{cc}) temperatures. The PLA crystallinity of the samples was determined according to Equation 2 [22]:

$$X_c = \frac{(\Delta Hm - \Delta Hcc)}{\Delta H_f \times X_{PLA}} . 100 \quad (2)$$

where ΔH_m and ΔH_{cc} are the enthalpies of melting and cold crystallization, respectively, ΔH_f is the melting enthalpy of 100% crystalline PLA (93 J/g) [22], and X_{PLA} is the weight fraction of PLA in the composite.

Tensile-tested fractured samples were analysed using a Hitachi Regulus 8230 High-Resolution Scanning Electron Microscope (Tokyo, Japan) at 3 kV and a secondary electron detector. The samples were metalized with platinum in a Quorum Q150V plus sputter coater (Laughton, East Sussex, United Kingdom) prior to analysis. In addition, optical microscopy images of a 3D printed sample were taken using an Olympus optical microscope model BX53 after mounting them in epoxy resin, rough and fine grinding, and polishing with Streuers OP-U silica suspension (Copenhagen, Denmark).

3. Results and Discussion

3.1 Fibre characterization

Fibre physical characteristics and composition were found to change after each treatment (Figure 1 and Table 2). The dried raw harakeke fibre is light brown and composed of fibre bundles. After alkali treatment, the fibres became lighter in colour due to the removal of lignin. As expected, the 10NaOH fibre was lighter in colour than the 5NaOH fibre due to increased removal of lignin; the lignin content of 5NaOH was 3.37% and that of 10NaOH was 2.23%. After bleaching, the colour of the fibre became almost white with further removal of lignin from the fibre surface and due to changes in the structure of the residual lignin; during H_2O_2 bleaching, chromophore structures of lignin can be decomposed through oxidation of the carbonyl and quinoid structure of the lignin side chain [23].

Each of the treatments changed the cellulose and hemicellulose content in the fibre. Raw harakeke fibre contains 46% cellulose and 18.80% hemicellulose; the cellulose content increased to 77.30% after 5% NaOH treatment. 10NaOH fibre provided 88% cellulose and after bleaching cellulose content increased to 92%. The higher amount of cellulose content in fibre is expected to provide higher reinforcement efficiency and thermal stability in composites.

Fibre diameter and length changed with digestion and bleaching (Table 2). Raw harakeke fibre is composed of fibre bundles of many single fibres attached to each other containing substances known to include hemicellulose, pectin, lignin, and other non-cellulosic components; after alkali treatment, fibres were separated from each other and appeared to have undergone removal of surface layers. The average diameter measured for the raw fibre bundle was 280 μm whereas 5NaOH fibre has an average diameter of 9.5 μm and occasional fibre bundles were still present. In contrast, the diameter of 10NaOH fibre was found to be less than 5NaOH fibre (7.3 μm) which is attributed to the removal of a higher amount of lignin and hemicellulose and better separation of the fibre bundles.

The length of the raw harakeke fibre bundle was about 1.5 m which was cut to 300 mm before digestion. After digestion, the fibre length of 5NaOH was found to be 1.60 mm and 1.38 mm for 10NaOH. There was a further drop in fibre length after bleaching, resulting in an average fibre length of 1.29 mm. Although there was a slight reduction of fibre length from 5NaOH to 10NaOH, the aspect ratio was found to be higher for 10NaOH compared to 5NaOH. The bleached fibre shows a similar aspect ratio to 10NaOH. It can be noted that the average length of treated fibre is well above the critical fibre length (L_c) found for some common natural fibre/polymer composites [24] which suggests that all the treated

fibre can act as reasonably efficient reinforcement. However, the reinforcing efficiency is expected to vary for different treated fibres due to different surface morphology and surface chemistry.

The surfaces of treated and untreated fibres were examined by SEM and are presented in Figure 2. The raw fibre surface is composed of lignin and other non-cellulosic components which results in a rough and uneven surface (see Fig. 2a). After alkali treatment, the fibre bundles are separated into elementary fibres and the fibre surface appeared to be much more even due to the removal of non-cellulosic components (Fig. 2b). Bleaching further removes residual lignin and as a result, the microfibril on the fibre surface can be seen clearly (white arrow in Fig.2c). When the bleached fibre was exposed to ultrasonication, the fibre became rougher with the appearance of microfibrils (yellow arrow) on its surface (See 2d). After 90 min of sonication treatment, the fibre surface is seen to have several long microfibrils (marked by a yellow arrow in Fig2e); however, some cracks on the surface are visible as marked by red arrows (Fig. 2f) and may be due to localized damage as a result of the excessive sonication effect.

The XRD diffractograms, TGA and DTG (derivative of the TG curve) thermograms of untreated and selected treated harakeke fibres are illustrated in supplementary (Figures S2 and S3) and the extracted data is presented in Table 3. The main XRD peaks attributed to crystalline cellulose Iβ ($2\theta \approx 16$ and 22.5^{o}) can be seen for all the fibre types [25]. The influence of the amorphous cellulose can be observed in the diffracted intensity at $2\theta = 18\text{-}19^{o}$. It is noteworthy that the crystalline peak of the crystallographic (002) planes ($2\theta = 22.5^{o}$) of cellulose in the treated fibres is significantly higher than for the raw fibre. This increased crystalline peak intensity represents a higher degree of crystallinity of cellulose in the treated fibre (can be seen in Table 3), due to the removal of lignin and hemicellulose (see Table 2). The higher cellulose crystallite size in the treated fibres is believed to be due to transcrystallinity that might have occurred due to the rearrangement of cellulose after the removal of lignin and hemicellulose through fibre treatment.

Referring to the TGA curve (Figure S3), a general initial drop in weight is seen in all the fibre types from room temperature to about 110^{o}C, which is attributed to the release of absorbed moisture. This was followed by two-stage degradation of the raw fibre, whereas the treated fibres exhibit one stage degradation. The two stages degradation in the raw fibre may be attributed to the decomposition of amorphous hemicellulose and lignin followed by the decomposition of the crystalline regions, which

would normally occur at a higher temperature than the amorphous regions. It is noteworthy that the observed degradation in the treated fibres falls in the same region as the second degradation stage of the raw fibre. This indicates that the hemicellulose and lignin components that induced first stage degradation in the raw fibre were significantly reduced in the treated fibres.

The onset temperature of thermal degradation occurred at a lower temperature for the raw fibre compared to the treated fibres. The higher onset temperature for treated fibres can be attributed to the significantly reduced amorphous components, i.e. hemicellulose, lignin, and other non-cellulosic components. The higher residue recorded at 600 ^{o}C for the raw fibre compared to treated fibre (see Table 3) further confirms the removal of lignin and other non-cellulosic impurities which contribute to the ash content.

3.2 Characterization of filaments and 3D printed composites

Images of the filaments obtained using a stereo microscope are presented in Figure 3. The diameter of the filaments was 1.70 ± 0.10 mm. The 5NaOH filament presented the roughest surface and the rest of the filaments were found to be smoother. The filaments produced with 5NaOH and 10NaOH fibre had the darkest colours whereas the bleached and ultrasonicated fibre composite surfaces were much lighter and smoother, which is attributed to the removal of residual lignin from the fibre surface and absence of fibre bundles.

The main properties obtained from TGA, onset temperature of degradation (T_{onset}) and temperature of maximum degradation rate (T_d), of neat PLA and the composite filaments are presented in Table 4. The TGA and DTG curves for all the conditions can be seen in Figure S4. Generally, PLA shows slightly higher thermal stability compared to all filaments. Amongst the composite filaments, bleached and ultrasonication treated fibre composite filaments exhibited higher thermal stability compared to 5NaOH and 10NaOH filaments. This is most likely to be due to the removal of less thermally stable non-cellulosic compounds (as can be seen in the low T_{onset} for raw and 5NaOH fibre in Table 3). It could also be a result of more ordered crystalline fibre in the bleached and ultrasonication treated fibre. Nevertheless, it can be seen that all the filaments are thermally stable at the printing temperature (210 ^{o}C) and there was no apparent degradation of the printed composites as evidenced by the similar colour of printed samples (Figure 4) and filaments (Figure 3).

The composite filaments were used to 3D print samples for tensile and DMA testing. Before printing, the printing conditions were adjusted to obtain samples with high surface quality. Although high fibre loading was used (30 wt%), all the samples were successfully printed without nozzle blockage (clogging). In addition, the composites presented excellent printability, especially the ones with bleached and sonicated fibres. Interestingly, it was possible to print all the samples using the same printing parameters of neat PLA, which is an important attribute for fibre-reinforced composites. In general, printing problems are reported when high fibre loading is used (above 20%) in the composites. This is often attributed to the increased viscosity of the molten composite, which generally results in clogging of the printer nozzle and making extrusion non-uniform [9,26,27].

The stress-strain behaviour of PLA and PLA composites containing different treated fibre (representative samples) is presented in Fig. 4, while the average ultimate tensile strength (UTS), Young's modulus (E) and elongation at break (ε_{break}) are summarised in Table 5. It can be seen that the UTS and E of the composites are higher for all the different treated fibres except 5NaOH than neat PLA. The composites with bleached fibres had considerably higher UTS and E compared to 10NaOH. This improvement is believed to be mainly related to the removal of non-cellulosic components from the fibre surface, and the breakage of the fibre bundles into elementary fibres. This would undoubtedly increase the fibre surface area and roughness, thereby exposing more OH groups for effective hydrogen bonding with PLA and improving the interface.

Ultrasonication treatment resulted in a noticeable increase in UTS and E values for 20 min and 40 min ultrasonication exposure times. It is believed that the rougher surface and presence of microfibrils on the surface of the ultrasonication-treated fibre, as seen in the SEM image (Fig. 2) would have facilitated a better fibre matrix interface to produce a significant increase in the UTS and E. However, when the ultrasonication exposure time was raised to 90 min, a significant decrease in the UTS and E values was observed. Hence, the drop in UTS and E for 90 min ultrasonication treated fibre composite could be due to possible damage to the fibre (some cracking has been identified on ultra -90 fibre surface -in Fig 2f) due to a longer period of sonication. A similar observation was reported in the literature regarding the adverse effect of ultrasonication treatment on natural fibres after extended exposure times. Based on this result, it can be inferred that the combination of ultrasonication treatment with other treatment methods can result in significant improvement in the mechanical properties of the resulting

composite. Nevertheless, it is noteworthy that prolonged exposure to ultrasonication can damage the fibre, and adversely affect the mechanical properties of the composite. Among all the composites, the ultra-40 formulation presented the highest UTS and E which are 21% and 150% higher than neat PLA respectively. The obtained tensile properties, i.e. UTS=79.3 MPa and E=8.7 GPa, are higher than the values previously reported for short fibre-reinforced 3D printed composites which generally vary between 15-57 MPa (UTS) and 1-4.4 GPa (E) [28–33]. To the best of our knowledge, the only study with similar results to our composites used 30 wt% of nanofibrillated cellulose (CNF), achieving a tensile strength of 80 MPa and Young's modulus of 7.1 GPa in 3D printed samples with similar geometry to our study [34]. It is worth mentioning that the obtained values are also higher than 3D printed PLA reinforced with short carbon fibres and glass fibres, which have TS and E between 44 - 60 MPa and 2.1- 4.8 GPa, respectively [35–37].

The authors believe that the performance achieved is due to the high printing quality, good interlayer adhesion, good dispersion and fibre orientation in the printing direction as can be seen in Figure 5. Figure 5a shows the side view of the printed sample where a good interlayer adhesion is apparent except for a few interlayer defects (as marked by the white arrows), common in 3D printed parts. Good fibre dispersion and preferred orientation of the fibres with the printing direction (longitudinal axis) can be observed in Figures 5b and 5c. In Figure 5c, it is possible to identify the cross-section of most of the fibres, which confirms the alignment of the fibres with the printing direction. The alignment of the fibres is induced by the extrusion during filament production and further encouraged during printing.

The elongation at break (EB) of the composites (Table 5 and Figure 4) was found to be lower than neat PLA, regardless of the type of fibre treatment. This is not unexpected, but it is interesting to note that 5NaOH fibre composite provided lower EB compared to 10NaOH fibre composite. This is potentially due to the lower interfacial strength due to the presence of fibre bundles, which act as a void thus reducing the EB. A decrease in EB observed for the bleached and ultrasonicated fibre composites is likely due to the reduction of fibre length and also due to the strong interface allowing crack propagation.

Tensile fracture surfaces of selected composite samples are presented in Figure 6. Figures 6a and 6c show entire fracture surfaces. Interlayer defects (marked by the orange arrow) can be seen and are relatively more pronounced in the 5NaOH formulation than the bleached fibre composites which may be due to the presence of fibre bundles, adversely affecting interlayer adhesion. Nevertheless, moderate

amounts of plastic deformation can be seen in good agreement with the stress-strain behaviour presented in Figure 4. In general, all the fracture surfaces have fibre fracture and fibre pull-out evidenced, however depending on the fibre treatment, the amount is varied. For example, more fibre pull-out can be seen for 5NaOH compared to bleached fibre composites (Figure 6b and 6d).

A few voids can be seen in Figure 6b as marked by the red arrow which is likely to be due to the pull-out of fibre bundles. On the other hand, for bleached fibre composites, this type of hole is almost absent possibly due to better dispersion of elementary fibres in the matrix. Some single fibre pull-out can be observed in most of the cases marked by white dotted arrows, however, the number of single fibre pull-out varies for different fracture surfaces. Increased fibre breakage, (Figure 6d compared to Figure 6b), indicated by the white arrows, suggests better interfacial bonding between the fibre and the matrix. This observation explains the higher UTS and E of bleached fibre composites compared to alkali-treated fibre composites. The amount of fibre breakage close to the main fracture path is increased for 40 min ultrasonication treated fibre composites (Figure 6e and 6f) which suggests good fibre wetting (yellow dotted arrow) and a stronger interface between the fibre and the matrix and accounts for the maximum UTS and E was observed (Table 5). A strong interface would be encouraged by the presence of microfibrils and fibre surface roughness due to sonication. A good interface can be observed for Ultra-90 as well, where good fibre wetting and fibre breakage can be seen but it can be observed that the broken fibre leaves a long path on the fracture surface. This is due to the localized fibre damage/stress concentration as a result of a longer period of sonication as shown in Fig. 2f. Premature fibre failure is likely to be responsible for the drastic reduction of tensile UTS and E of 90 min ultrasonication treated fibre composites.

3.3 Thermo-mechanical stability and DSC analysis

Thermomechanical properties of 3D printed samples in the temperature range of 25–140 °C were studied using DMA. Storage modulus and tan δ against temperature plots are shown in Figure 7. Storage modulus reflects the mechanical energy stored by samples during a loading cycle and it is related to the stiffness and shape recovery of the polymer during the unloading process. Reinforcing PLA with fibres generally improves its thermo-mechanical properties, which can broaden its applications where thermo-mechanical stability is necessary [34,38–40]. Incorporating harakeke fibre generally increased the storage modulus of PLA, more than doubling it at room temperature with the 40 min ultrasonication treated fibre

formulation. The storage modulus of the differently treated fibre composites was found to follow a similar trend as Young's modulus obtained by static tensile testing. A summary of the storage modulus at different temperatures, tan δ, and T_g is given in Table 6. One of the main advantages of adding the harakeke fibres is the increase of storage modulus at higher temperatures, which for Ultra-40 sample was almost 6 times higher at 60°C than neat PLA. Tan δ is the ratio between loss modulus (E'') and storage modulus (E'), which is used to identify the glassy to rubbery transition and the temperature of its maximum is often used as the glass transition (T_g) temperature. The intensity of the tan δ peak (max tan δ) was considerably reduced with the addition of harakeke fibres, which indicates less viscous behaviour and better thermomechanical stability.

The 3D printed samples used for tensile testing were also analysed by DSC to verify the thermophysical properties of the composites. The DSC curves for the first and second heating cycles of printed samples are shown in the supplementary Figure S6 and the corresponding data derived from the DSC analyses are given in Table 7. All the samples have a typical DSC curve for the 2003D PLA grade, with an endothermic T_g (glass transition temperature) peak at 60-64 °C, an exothermic T_{cc} (cold crystallization temperature) peak between 114-120 °C and an endothermic T_m (melting temperature) peak between 150-152 °C.

The first thing to notice is that all the samples with fibres presented a lower T_{cc} temperature and higher PLA crystallinity. Although this PLA grade (2003D) has high D-isomer content and does not crystallise during cooling [41], the printing process causes a temperature gradient in the sample which may induce crystallisation in PLA, especially in the presence of fibres. This effect corroborates with the decrease in temperature with the addition of fibres for the initial increase of storage modulus caused by crystallisation observed in the DMA results. In addition, some of the composite samples present two peaks of fusion (indicated in Figure S5 of the supplementary file) that is related to the melting of the disordered and metastable α form of PLA (α') potentially formed during 3D printing [41–45]. In this case, the first peak of fusion is related to the simultaneous melting of the primary α crystals formed during printing (and during the heating cycle) and recrystallisation of α' to α crystal form. The second peak of fusion is attributed to the melting of α crystal form generated in the recrystalisation process [46]. The T_g in the first heating cycle is similar to the T_g values obtained by DMA analysis and in general, the

composite samples presented higher values than neat PLA, which can be attributed to the higher crystallinity of PLA in these samples.

Interestingly, the second heating cycle shows that all the samples have similar behaviour, showing low values of crystallinity (since this PLA grade does not crystallise upon cooling), and similar values of T_g, T_{cc}, and T_m. Although the fibres facilitate the crystallisation of PLA during the printing process, in controlled heating/cooling conditions (used in the DSC) they do not have a strong influence on the thermo-physical behaviour of PLA. In the printing process, there are considerable gradients of temperature and heating/cooling rates, which combined with the presence of fibres, can have more influence on the crystallisation process of PLA.

4 Conclusions

In this work, harakeke microfibres produced by alkaline and bleaching treatments followed by a surface modification using ultrasonication were used in the production of PLA-based composites for 3D printing using fused deposition modelling. Alkaline digestion followed by bleaching of harakeke fibres (New Zealand flax) resulted in elementary fibres with high cellulose content (92 wt%), and an average diameter and length of 7-9 µm and 1.3-1.6 mm, respectively. With ultrasonication of the bleached fibres, defibrillation was induced and microfibrils appeared on the fibre surface. The combined approach of using chemical and physical fibre treatments enabled the production of PLA-based composite filaments for 3D printing with high fibre content without compromising printability and surface quality. PLA composites produced by 3D printing with 30 wt% of fibres had higher tensile strength and Young's modulus than neat PLA, achieving maximum values of 79.3 MPa and 8.7 GPa, respectively, using fibres treated by ultrasonication for 40 min. The tensile properties found in this study were higher than in any other study conducted using similar short fibres for PLA composites. In addition, the fibres were well dispersed and showed preferred orientation to the printing direction. Microfibril and surface roughness through ultrasonication improves interfacial bonding between the fibre and the matrix. The addition of fibres also improved the thermo-mechanical stability of 3D printed samples, increasing the storage modulus at higher temperatures (4.5x higher than neat PLA at 60 ºC) and considerably decreasing the maximum tan δ.

Acknowledgements

The authors would like to thank the financial support from the Ministry of Business, Innovation and Employment (MBIE) New Zealand Endeavour Fund, through the project Āmiomio Aotearoa – A circular Economy for the wellbeing of New Zealand (UOWX2004) and the National Science Challenge spearhead project "Additive manufacturing and 3D and/or 4D printing of bio-composites" [grant 2019-S5-CRS].

References

[1] Chacón JM, Caminero MA, Núñez PJ, García-Plaza E, García-Moreno I, Reverte JM. Additive manufacturing of continuous fibre reinforced thermoplastic composites using fused deposition modelling: Effect of process parameters on mechanical properties. Compos Sci Technol 2019;181:107688. https://doi.org/10.1016/j.compscitech.2019.107688.

[2] Melenka GW, Cheung BKO, Schofield JS, Dawson MR, Carey JP. Evaluation and prediction of the tensile properties of continuous fiber-reinforced 3D printed structures. Compos Struct 2016;153:866–75. https://doi.org/10.1016/j.compstruct.2016.07.018.

[3] Bi H, Ren Z, Guo R, Xu M, Song Y. Fabrication of flexible wood flour/thermoplastic polyurethane elastomer composites using fused deposition molding. Ind Crops Prod 2018;122:76–84. https://doi.org/10.1016/j.indcrop.2018.05.059.

[4] Peng Y, Wu Y, Li S, Wang K, Yao S, Liu Z, et al. Tailorable rigidity and energy-absorption capability of 3D printed continuous carbon fiber reinforced polyamide composites. Compos Sci Technol 2020;199:108337. https://doi.org/10.1016/j.compscitech.2020.108337.

[5] Gauss C, Pickering K, Muthe LP. The use of cellulose in bio-derived formulations for 3D/4D printing: a review. Compos Part C Open Access 2021;4:100113. https://doi.org/10.1016/j.jcomc.2021.100113.

[6] Aydın M, Tozlu H, Kemaloglu S, Aytac A, Ozkoc G. Effects of Alkali Treatment on the Properties of Short Flax Fiber-Poly(Lactic Acid) Eco-Composites. J Polym Environ 2011;19:11–7. https://doi.org/10.1007/s10924-010-0233-9.

[7] Xiao X, Chevali VS, Song P, He D, Wang H. Polylactide/hemp hurd biocomposites as sustainable 3D printing feedstock. Compos Sci Technol 2019;184:107887. https://doi.org/10.1016/j.compscitech.2019.107887.

[8] Milosevic M, Stoof D, Pickering K. Characterizing the Mechanical Properties of Fused Deposition Modelling Natural Fiber Recycled Polypropylene Composites. J Compos Sci 2017;1:7. https://doi.org/10.3390/jcs1010007.

[9] Stoof D, Pickering K, Zhang Y. Fused Deposition Modelling of Natural Fibre/Polylactic Acid Composites. J Compos Sci 2017;1. https://doi.org/10.3390/jcs1010008.

[10] Pickering KL, Efendy MGA, Le TM. A review of recent developments in natural fibre composites and their mechanical performance. Compos Part A Appl Sci Manuf 2016;83:98–112. https://doi.org/10.1016/j.compositesa.2015.08.038.

[11] Bogoeva-Gaceva G, Avella M, Malinconico M, Buzarovska A, Grozdanov A, Gentile G, et al. Natural fiber eco-composites. Polym Compos 2007;28:98–107. https://doi.org/10.1002/pc.20270.

[12] Cordeiro N, Gouveia C, Moraes a. GO, Amico SC. Natural fibers characterization by inverse gas chromatography. Carbohydr Polym 2011;84:110–7. https://doi.org/10.1016/j.carbpol.2010.11.008.

[13] Alao PF, Press R, Kallakas H, Ruponen J, Poltimäe T, Kers J. Investigation of Efficient Alkali Treatment and the Effect of Flame Retardant on the Mechanical and Fire Performance of Frost-Retted Hemp Fiber Reinforced PLA. Polymers (Basel) 2022;14:2280. https://doi.org/10.3390/polym14112280.

[14] Dowling NE. Mechanical Behavior of Materials. 4th ed. Pearson Education; 2013.

[15] Krishnaiah P, Ratnam CT, Manickam S. Enhancements in crystallinity, thermal stability, tensile modulus and strength of sisal fibres and their PP composites induced by the synergistic effects of alkali and high intensity ultrasound (HIU) treatments. Ultrason Sonochem 2017;34:729–42. https://doi.org/10.1016/j.ultsonch.2016.07.008.

[16] Tischer PCSF, Sierakowski MR, Westfahl H, Tischer CA. Nanostructural reorganization of bacterial cellulose by ultrasonic treatment. Biomacromolecules 2010;11:1217–24. https://doi.org/10.1021/bm901383a.

[17] Iskalieva A, Yimmou BM, Gogate PR, Horvath M, Horvath PG, Csoka L. Cavitation assisted delignification of wheat straw: A review. Ultrason Sonochem 2012;19:984–93. https://doi.org/10.1016/j.ultsonch.2012.02.007.

[18] Renouard S, Hano C, Doussot J, Blondeau JP, Lainé E. Characterization of ultrasonic impact on coir, flax and hemp fibers. Mater Lett 2014;129:137–41. https://doi.org/10.1016/j.matlet.2014.05.018.

[19] Moshiul Alam AKM, Beg MDH, Reddy Prasad DM, Khan MR, Mina MF. Structures and performances of simultaneous ultrasound and alkali treated oil palm empty fruit bunch fiber reinforced poly(lactic acid) composites. Compos Part A Appl Sci Manuf 2012;43:1921–9. https://doi.org/10.1016/j.compositesa.2012.06.012.

[20] Pettersen RC. Wood Sugar Analysis by Anion Chromatography. J Wood Chem Technol 1991;11:495–501. https://doi.org/10.1080/02773819108051089.

[21] Nam S, French AD, Condon BD, Concha M. Segal crystallinity index revisited by the simulation of X-ray diffraction patterns of cotton cellulose Iβ and cellulose II. Carbohydr Polym 2016;135:1–9. https://doi.org/10.1016/j.carbpol.2015.08.035.

[22] Pilla S, Gong S, O'Neill E, Rowell RM, Krzysik AM. Polylactide-pine wood flour composites. Polym Eng Sci 2008;48:578–87. https://doi.org/10.1002/pen.20971.

[23] Wu Y, Wu J, Yang F, Tang C, Huang Q. Effect of H2O2 bleaching treatment on the properties of finished transparent wood. Polymers (Basel) 2019;11:1–13. https://doi.org/10.3390/polym11050776.

[24] Aliotta L, Lazzeri A. A proposal to modify the Kelly-Tyson equation to calculate the interfacial shear strength (IFSS) of composites with low aspect ratio fibers. Compos Sci Technol 2020;186:107920. https://doi.org/10.1016/j.compscitech.2019.107920.

[25] Driemeier C. Two-dimensional Rietveld analysis of celluloses from higher plants. Cellulose 2014;21:1065–73. https://doi.org/10.1007/s10570-013-9995-2.

[26] Ahmad Adlie Shamsuri *. Important Criteria for Preparation of 3D Printer Filaments from Polymer Biocomposites . SVOA Mater Sci Technol 2019;1:1–3.

[27] Tarrés Q, Melbø JK, Delgado-Aguilar M, Espinach FX, Mutjé P, Chinga-Carrasco G. Bio-polyethylene reinforced with thermomechanical pulp fibers: Mechanical and micromechanical characterization and its application in 3D-printing by fused deposition modelling. Compos Part B Eng 2018;153:70–7. https://doi.org/10.1016/j.compositesb.2018.07.009.

[28] Fused Deposition Modelling of Natural Fibre/Polylactic Acid Composites. J Compos Sci 2017;1:8. https://doi.org/10.3390/jcs1010008.

[29] Depuydt D, Balthazar M, Hendrickx K, Six W, Ferraris E, Desplentere F, et al. Production and characterization of bamboo and flax fiber reinforced polylactic acid filaments for fused deposition modeling (FDM). Polym Compos 2019;40:1951–63. https://doi.org/10.1002/pc.24971.

[30] Liu H, He H, Peng X, Huang B, Li J. Three-dimensional printing of poly(lactic acid) bio-based composites with sugarcane bagasse fiber: Effect of printing orientation on tensile performance. Polym Adv Technol 2019;30:910–22. https://doi.org/10.1002/pat.4524.

[31] Zhao X, Tekinalp H, Meng X, Ker D, Benson B, Pu Y, et al. Poplar as Biofiber Reinforcement in Composites for Large-Scale 3D Printing. ACS Appl Bio Mater 2019. https://doi.org/10.1021/acsabm.9b00675.

[32] Filgueira D, Holmen S, Melbø JK, Moldes D, Echtermeyer AT, Chinga-Carrasco G. Enzymatic-Assisted Modification of Thermomechanical Pulp Fibers to Improve the Interfacial Adhesion with Poly(lactic acid) for 3D Printing. ACS Sustain Chem Eng 2017;5:9338–46. https://doi.org/10.1021/acssuschemeng.7b02351.

[33] Antony S, Cherouat A, Montay G. Fabrication and Characterization of Hemp Fibre Based 3D Printed Honeycomb Sandwich Structure by FDM Process. Appl Compos Mater 2020. https://doi.org/10.1007/s10443-020-09837-z.

[34] Tekinalp HL, Meng X, Lu Y, Kunc V, Love LJ, Peter WH, et al. High modulus biocomposites via additive manufacturing: Cellulose nanofibril networks as “microsponges.” Compos Part B Eng 2019;173:106817. https://doi.org/10.1016/j.compositesb.2019.05.028.

[35] Maqsood N, Rimašauskas M. Characterization of carbon fiber reinforced PLA composites manufactured by fused deposition modeling. Compos Part C Open Access 2021;4. https://doi.org/10.1016/j.jcomc.2021.100112.

[36] Li Y, Gao S, Dong R, Ding X, Duan X. Additive Manufacturing of PLA and CF/PLA Binding Layer Specimens via Fused Deposition Modeling. J Mater Eng Perform 2018. https://doi.org/10.1007/s11665-017-3065-0.

[37] Rahimizadeh A, Kalman J, Fayazbakhsh K, Lessard L. Recycling of fiberglass wind turbine blades into reinforced filaments for use in Additive Manufacturing. Compos Part B Eng 2019. https://doi.org/10.1016/j.compositesb.2019.107101.

[38] Tingaut P, Zimmermann T, Lopez-Suevos F. Synthesis and characterization of bionanocomposites with tunable properties from poly(lactic acid) and acetylated microfibrillated cellulose. Biomacromolecules 2010;11:454–64. https://doi.org/10.1021/bm901186u.

[39] Li N, Li Y, Liu S. Rapid prototyping of continuous carbon fiber reinforced polylactic acid composites by 3D printing. J Mater Process Technol 2016;238:218–25. https://doi.org/10.1016/j.jmatprotec.2016.07.025.

[40] Jonoobi M, Harun J, Mathew AP, Oksman K. Mechanical properties of cellulose nanofiber (CNF) reinforced polylactic acid (PLA) prepared by twin screw extrusion. Compos Sci Technol 2010;70:1742–7. https://doi.org/10.1016/j.compscitech.2010.07.005.

[41] Coppola B, Cappetti N, Maio L Di, Scarfato P, Incarnato L. 3D printing of PLA/clay nanocomposites: Influence of printing temperature on printed samples properties. Materials (Basel) 2018;11. https://doi.org/10.3390/ma11101947.

[42] Liao Y, Liu C, Coppola B, Barra G, Di Maio L, Incarnato L, et al. Effect of porosity and crystallinity on 3D printed PLA properties. Polymers (Basel) 2019;11:1–14. https://doi.org/10.3390/polym11091487.

[43] Jiang L, Shen T, Xu P, Zhao X, Li X, Dong W, et al. Crystallization modification of poly(lactide) by using nucleating agents and stereocomplexation. E-Polymers 2016;16:1–13. https://doi.org/doi:10.1515/epoly-2015-0179.

[44] Farah S, Anderson DG, Langer R. Physical and mechanical properties of PLA, and their functions in widespread applications — A comprehensive review. Adv Drug Deliv Rev 2016;107:367–92. https://doi.org/https://doi.org/10.1016/j.addr.2016.06.012.

[45] Nassar A, Younis M, Elzareef M, Nassar E. Effects of heat-treatment on tensile behavior and dimension stability of 3d printed carbon fiber reinforced composites. Polymers (Basel) 2021;13:1–21. https://doi.org/10.3390/polym13244305.

[46] Tábi T, Hajba S, Kovács JG. Effect of crystalline forms (α′ and α) of poly(lactic acid) on its mechanical, thermo-mechanical, heat deflection temperature and creep properties. Eur Polym J 2016;82:232–43. https://doi.org/10.1016/j.eurpolymj.2016.07.024.

REVISED Manuscript (revised text UNMARKED)

Click here to view linked References

Graphical Abstract

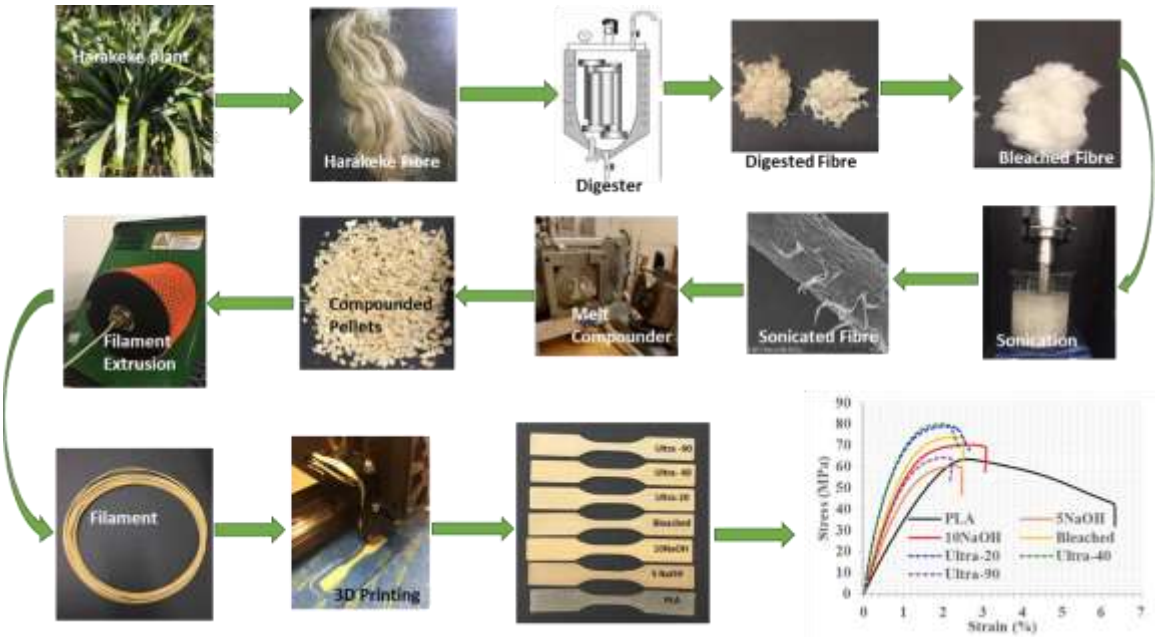

Highlights:

- Harakeke microfibres with cellulose content of 92 wt% were produced.
- Fibres were well dispersed and aligned to the printing direction in 3D printed samples.
- Fibre/matrix interfacial bonding improved with ultrasonication treatment.
- Tensile strength of 79 MPa and Young's modulus of 8.7 GPa achieved in 3D printed samples.
- The addition of fibres improved the thermo-mechanical stability of the composites.